RESEARCH

Assessment of androgen receptor expression in breast cancer patients using 18 F-FDG PET/CT radiomics and clinicopathological characteristics

Tongtong Jia[1†], Qingfu Lv[2†], Bin Zhang[1†], Chunjing Yu[3*], Shibiao Sang[1*] and Shengming Deng[1*]

Abstract

Objective   In the present study, we mainly aimed to predict the expression of androgen receptor (AR) in breast cancer (BC) patients by combing radiomic features and clinicopathological factors in a non-invasive machine learning way.

Materials and methods   A total of 48 BC patients, who were initially diagnosed by ^{18}F-FDG PET/CT, were retrospectively enrolled in this study. LIFEx software was used to extract radiomic features based on PET and CT data. The most useful predictive features were selected by the LASSO (least absolute shrinkage and selection operator) regression and t-test. Radiomic signatures and clinicopathologic characteristics were incorporated to develop a prediction model using multivariable logistic regression analysis. The receiver operating characteristic (ROC) curve, Hosmer-Lemeshow (H-L) test, and decision curve analysis (DCA) were conducted to assess the predictive efficiency of the model.

Results   In the univariate analysis, the metabolic tumor volume (MTV) was significantly correlated with the expression of AR in BC patients (p < 0.05). However, there only existed feeble correlations between estrogen receptor (ER), progesterone receptor (PR), and AR status (p = 0.127, p = 0.061, respectively). Based on the binary logistic regression method, MTV, SHAPE_Sphericity$_{CT}$ (CT Sphericity from SHAPE), and GLCM_Contrast$_{CT}$ (CT Contrast from grey-level co-occurrence matrix) were included in the prediction model for AR expression. Among them, GLCM_Contrast$_{CT}$ was an independent predictor of AR status (OR = 9.00, p = 0.018). The area under the curve (AUC) of ROC in this model was 0.832. The p-value of the H-L test was beyond 0.05.

[†]Tongtong Jia, Qingfu Lv, and Bin Zhang contributed equally to this work.

*Correspondence:
Chunjing Yu
chunjingyu2022@163.com
Shibiao Sang
sshibiao@163.com
Shengming Deng
dshming@163.com
Full list of author information is available at the end of the article

Conclusions A prediction model combining radiomic features and clinicopathological characteristics could be a promising approach to predict the expression of AR and noninvasively screen the BC patients who could benefit from anti-AR regimens.

Keywords Breast cancer, Androgen receptor, Radiomics, ^{18}F-FDG PET/CT, Clinicopathological, Machine learning

Introduction

Breast cancer (BC) has already become the most frequently diagnosed tumor and the leading cause of cancer-related death among women worldwide [1, 2]. According to the different expressions of specific molecular receptors, BC can be classified into various subtypes, which are tightly associated with the treatment strategy selection and prognosis [3, 4]. However, even with classic targeted therapies, a certain proportion of patients are insensitive to treatments and develop varying degrees of resistance [5–8]. Therefore, more attention should be paid to new molecular targets to assist in the diagnosis and treatment of BC.

Most recent studies have investigated the roles of androgen receptor (AR) in BC patients, showing that AR has different subtypes with considerable levels of expression [9, 10]. AR and estrogen receptor (ER) competitively bind to estrogen-dependent signaling pathways, and this crosstalk may contribute to acquired resistance to endocrine therapy [11, 12]. Besides, the expression of AR is highly correlated with the amplification of human epidermal growth factor 2 (HER2), which is coupled with AR activation and enhances the oncogenic function of certain signaling pathways [13, 14]. Triple-negative BC (TNBC) lacks recognized molecular targets, in which the expression of AR is related to ER-regulated gene transcription and a lower rate of pathological complete response (pCR) to neoadjuvant chemotherapy [15, 16]. Consequently, early recognition of AR expression not only helps predict prognosis but also guides the application of AR-targeted therapy, effectively improving patients' sensitivity to traditional therapies and prolonging their overall survival.

At present, the expressions of molecular receptors are generally detected through immunohistochemistry (IHC). Such an approach is mainly based on biopsy as an invasive procedure, and it is rarely repeatable and unrepresentative due to small tissue samples and intratumor heterogeneity [17]. ^{18}F-FDG PET/CT (Fluorine-18 fluorodeoxyglucose positron emission tomography/computed tomography), which combines functional metabolic quantification and morphological imaging, is commonly used for initial staging, post-treatment assessment and re-staging in BC [18, 19]. Radiomics, which uses medical imaging to noninvasively quantify intratumoral heterogeneity, has emerged as a translational research topic in BC [20]. Recent literature has indicated that radiomic features obtained from ^{18}F-FDG PET/CT can contribute to the prediction of tumor molecular subtypes, while there are still limited studies focusing on the role of AR as a predictive parameter [17].

In the present study, we aimed to develop a machine-learning model for individual prediction of AR expression in BC patients by exploring the correlations between radiomic features, clinicopathological factors, and AR status. In addition, our findings might help identify the patients who could benefit from the AR-targeted treatment.

Materials and methods

Patients

This retrospective study was approved by the institutional review board of the First Affiliated Hospital of Soochow University, and the informed consent was waived because of its retrospective nature. Our current study was conducted in accordance with the Declaration of Helsinki, and the trial registration number of this study was ChiCTR2200062858.

All patients were histologically diagnosed as primary BC and underwent ^{18}F-FDG PET/CT imaging for staging between December 2017 and April 2022. The specific inclusion criteria were as follows: (1) aged beyond 18 years; (2) without any therapy before the standard examination of ^{18}F-FDG PET/CT; (3) with histological data (type and grade) derived from biopsy (generally for large lesions) or surgical specimens (routinely for relatively smaller lesions); (4) with IHC examination of AR performance; and (5) with complete clinical and imaging datasets. Exclusion criteria were as follows: (1) without complete ^{18}F-FDG PET/CT images or good imaging quality; (2) with the too-small size of the primary lesion for segmentation; (3) with multiple lesions of BC; (4) with other types of cancers; and (5) with unclear histological proof.

^{18}F-FDG PET/CT imaging

The patients were injected ^{18}F-FDG (4.07–5.55 MBq/kg) for routine preparation after fasting for at least 6 h to ensure the blood glucose level was below 11.1 mmol/L. Approximately 40–60 min later, an integrated PET/CT scanner (Discovery STE, General Electric Medical Systems, Milwaukee, WI, USA) was adopted to acquire images from the base of the skull to the midthigh. With the acquisition parameters (transaxial field of view of 70 cm, pitch of 1.75, rotation time of 0.8 s, and slice thickness of 3.75 mm), low-dose (140 kV, 120 mA) CT
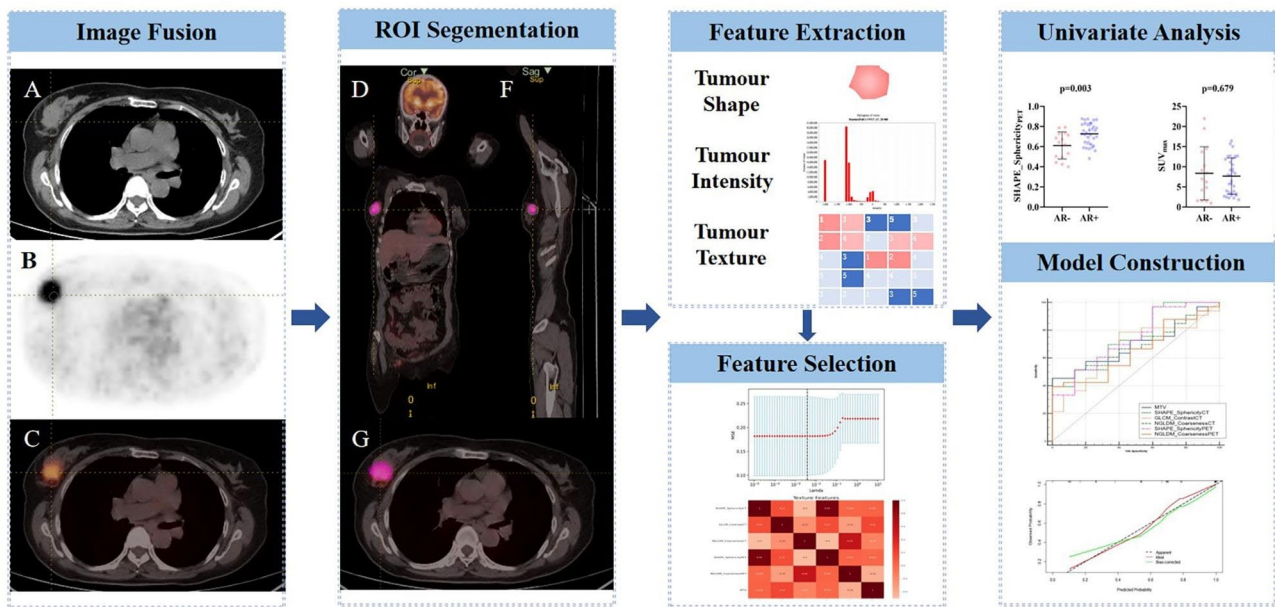
Fig. 1 The workflow of this study. CT image (**A**), PET image (**B**), PET/CT fusion image (**D**), coronary image (**E**), sagittal image (**F**), and transaxial image (**G**) of ^{18}F-FDG PET/CT display an example of VOI for extracting imaging features of BC. A patient with stage IV of BC underwent PET/CT image showing a metabolically active right breast lesion

images were acquired for the following attenuation correction and anatomic localization. Immediately, PET image acquisition was performed for 2–3 min per bed position. Finally, the ordered subset expectation maximization algorithm was used for image reconstruction.

Pathological evaluation

Histological sections stained with hematoxylin and eosin (H&E staining) were observed under the microscope to confirm the histologic type and grade by two pathologists independently. The expressions of ER, PR, HER2, Ki-67, and AR were detected by IHC. More than 10% of tumor nuclei with positive AR staining were defined as AR positive (AR+) regardless of staining intensity, otherwise defined as AR negative (AR-). As for ER and PR, both proportional staining (%) and staining intensity (weak, medium, and strong) were considered. The combination of IHC scores (1+, 2+, and 3+) and fluorescence in situ hybridization (FISH) was used to determine HER2 status. Ki-67 was divided into high expression and low expression according to a cutoff value of 30% of positively stained cells.

Extraction and selection of radiomic features

After image acquisition, PET and CT images in the DICOM format were imported into LIFEx freeware (v7.0.0 https://www.lifexsoft.org/), which automatically fused them for quantitative PET/CT analysis [21]. Two experienced nuclear medicine physicians, each with over 15 years of diagnostic experience, manually segmented the three-dimensional volume of interest (VOI) on every slice of primary breast lesions and metastatic lymph nodes. They were blinded to the clinical and pathological outcomes, except for the presence of BC. The VOI was defined with a threshold of 40% of the maximum standardized uptake value (SUV_{max}), which included MTV and total lesion glycolysis (TLG). Intensity discretization for CT data was performed with the number of gray levels of 400 bins and absolute scale bounds from $-1,000$ to 3,000 HU. In contrast, it was segmented into 64 bins and measured with SUV_{max} ranging from 0 to 20 for PET images. Moreover, the radiomic features of PET and CT were calculated automatically by this software for texture analysis. Intra-class correlation coefficients (ICCs) were calculated to evaluate the repeatability of all the features, of which ICCs > 0.75 were selected for model construction. Subsequently, the least absolute shrinkage and selection operator (LASSO) regression algorithm and t-test were used for the selection of the remaining features. Finally, 10-fold cross-validation was used to ensure the robustness of the optimal features.

Construction and evaluation of the prediction model

Univariate regression analysis was used to screen out clinicopathological risk factors with statistically significant differences from potential predictors, including age, BMI, menopausal status, tumor location, histological types, clinical TNM staging, and molecular types. The above-mentioned risk factors were subsequently combined with radiomic features and analyzed

Table 1 Characteristics of included BC patients with different AR expression statuses

Characteristics	AR- (n = 15)	AR+ (n = 33)	$t/x^2/z$	p-value
Age (years)	56.00 ± 15.28	53.70 ± 13.74	0.520	0.606
BMI (kg/m^2)	24.69 ± 4.25	24.82 ± 4.02	0.100	0.921
Menopausal Status			0.162	0.688
Premenopausal	5(33.3%)	13(39.4%)		
Postmenopausal	10(66.7%)	20(60.6%)		
Tumor Location			0.014	0.907
Left	8(53.3%)	17(51.5%)		
Right	7(46.7%)	16(48.5%)		
Histologic Type			0.514	0.662
IDC	12(80.0%)	29(87.9%)		
Other	3(20.0%)	4(12.1%)		
Clinical Stage			0.730	0.393
I-II	4(26.7%)	13(39.4%)		
III-IV	11(73.3%)	20(60.6%)		
Clinical T Stage			0.183	0.738
T1-T2	10(66.7%)	24(72.7%)		
T3-T4	5(33.3%)	9(27.3%)		
Clinical N Stage			1.302	0.629
N0	4(26.7%)	14(42.4%)		
N1-2	6(40.0%)	9(27.3%)		
N3	5(33.3%)	10(30.3%)		
Clinical M Stage			0.032	1.000
M0	11(73.3%)	25(75.8%)		
M1	4(26.7%)	8(24.2%)		
ER Status			2.334	0.127
Positive	7(46.7%)	23(69.7%)		
Negative	8(53.3%)	10(30.3%)		
PR Status			3.499	0.061
Positive	3(20.0%)	16(48.5%)		
Negative	12(80.0%)	17(51.5%)		
HER2 Status			0.162	0.688
Positive	5(33.3%)	13(39.4%)		
Negative	10(66.7%)	20(60.6%)		
Molecular Subtype			3.232	0.337
HR+/HER2-	6(40.0%)	15(45.5%)		
HR+/HER2+	1(6.7%)	8(24.2%)		
HER2+	4(26.7%)	5(15.2%)		
TNBC	4(26.7%)	5(15.2%)		
Ki-67			0.041	0.839
<30%	5(33.3%)	12(36.4%)		
≥30%	10(66.7%)	21(63.6%)		
SUV$_{max}$	8.38 ± 6.61	7.70 ± 4.49	0.416	0.679
SUV$_{mean}$	2.66 ± 2.02	2,94 ± 1.91	-0.477	0.636
TLG*	62.00(19.11 ~ 126.26)	44.26(15.62 ~ 129.46)	-0.612	0.541
MTV*	35.50(20.83 ~ 64.00)	17.70 (8.70 ~ 47.53)	-2.146	0.032

*Those data are described as median (lower quartile ~ upper quartile) and tested by the Mann-Whitney U test. AR-, androgen receptor negative; AR+, androgen receptor positive; t: independent t-test; x^2, Chi-square test; z, Mann-Whitney U test; BMI: body mass index; ER, estrogen receptor; PR, progesterone receptor; HER2, human epidermal growth factor receptor-2; IDC, invasive ductal breast carcinoma; HR, hormone receptor (included ER and/or PR); TNBC, triple-negative breast cancer; Ki-67, cellular proliferation index; SUV$_{max}$, maximum standardized uptake value; SUV$_{mean}$, mean standardized uptake value; TLG, total lesion glycolysis; MTV, metabolic tumor volume

by multivariable logistic regression analysis to develop a prediction model. The receiver operating characteristic (ROC) curve, Hosmer-Lemeshow (H-L) test, and decision curve analysis (DCA) were used to evaluate the discrimination, calibration, and clinical usefulness of the model, respectively.

Jia *et al. BMC Medical Imaging*   (2023) 23:93

Page 5 of 11

Table 2 Radiomic parameters extracted from PET/CT images

Conventional	First-order	Higher-order			
		GLZLM	GLRLM	GLCM	NGLDM
SUV/HU_{min}	HISTO_Skewness	GLZLM_SZE (Short-Zone Emphasis)	GLRLM_SRE (Short-Run Emphasis)	GLCM_Homogeneity	NGLDM_ Coarseness
SUV/HU_{mean}	HISTO_Kurtosis	GLZLM_LZE (Long-Zone Emphasis)	GLRLM_LRE (Long-Run Emphasis)	GLCM_Energy	NGLDM_ Contrast
SUV/HU_{std}	HISTO_Entropy_log10	GLZLM_LGZE (Low Gray-level Zone Emphasis)	GLRLM_LGRE (Low Gray-level Run Emphasis)	GLCM_Contrast	NGLDM_ Busyness
SUV/HU_{max}	HISTO_Entropy_log2	GLZLM_HGZE (High Gray-level Zone Emphasis)	GLRLM_HGRE (High Gray-level Run Emphasis)	GLCM_Correlation	
SUV_{peak}*	HISTO_Energy	GLZLM_SZLGE (Short-Zone Low Gray-level Emphasis)	GLRLM_SRLGE (Short-Run Low Gray-level Emphasis)	GLCM_Entropy_log10	
TLG*	SHAPE_Sphericity	GLZLM_SZHGE (Short-Zone High Gray-level Emphasis)	GLRLM_SRHGE (Short-Run High Gray-level Emphasis)	GLCM_Entropy_log2	
	SHAPE_Compacity	GLZLM_LZLGE (Long-Zone Low Gray-level Emphasis)	GLRLM_LRLGE (Long-Run Low Gray-level Emphasis)	GLCM_Dissimilarity	
	SHAPE_Volume (mL)	GLZLM_LZHGE (Long-Zone High Gray-level Emphasis)	GLRLM_LRHGE (Long-Run High Gray-level Emphasis)		
	SHAPE_Volume(vx)	GLZLM_GLNU (Gray-Level Non-Uniformity for zone)	GLRLM_GLNU (Gray-Level Non-Uniformity for run)		
		GLZLM_ZLNU (Zone Length Non-Uniformity)	GLRLM_RLNU (Run Length Non-Uniformity)		
		GLZLM_ZP (Zone%)	GLRLM_RP (Run Percentage)		

*Calculated only for the PET data. SUV, standardized uptake value; TLG, total lesion glycolysis; HISTO, Histogram; GLZLM, Gray-Level Zone Length Matrix; GLRLM, Gray-Level Run Length Matrix; GLCM, Gray-Level Co-Occurrence Matrix; NGLDM, Neighboring Gray-level dependence matrix

Statistical analysis

All statistical data were calculated and analyzed with IBM SPSS statistics version 26.0, Python version 3.11 (https://www.python.org), MedCalc software (MedCalc Software, Ostend, Belgium), and R version 4.2.1 (http://www.R-project.org). The normality and homogeneity of variance of continuous data were evaluated by the Kolmogorov-Smirnov test and Levene's test, respectively. The numeric variables were tested by the independent t-test and Mann-Whitney U test. Instead, the Chi-square test and Fisher's exact test were applied to analyze categorical variables. $P < 0.05$ was considered statistically significant. Figure 1 presents the workflow of this study.

Results

Clinicopathologic characteristics

A total of 48 BC patients were included in our study. Table 1 shows the baseline characteristics of these patients. Among the 48 patients, 33 patients (68.75%) were histologically confirmed as AR+, while 15 patients (31.25%) were confirmed as AR-. In our univariate analysis, MTV was tightly relevant to the expression of AR (p=0.032). The ER and PR status were weakly correlated with AR status (p=0.127 and 0.061, respectively). However, there was no significant difference found across the other clinical characteristics between the AR+ and AR- groups.

Feature selection

Table 2 presents 80 radiomic features extracted from CT and PET datasets. Five features were considered valuable for the prediction of the AR expression using both the t-test and LASSO regression model. Figure 2 shows the most suitable Lambda parameter of LASSO regression. For the CT dataset, SHAPE_Sphericity$_{CT}$, GLCM_Contrast$_{CT}$, and NGLDM_Coarseness$_{CT}$ (CT Coarseness from neighborhood gray-level difference matrix) were selected. SHAPE_Sphericity$_{PET}$ (PET Sphericity from SHAPE) and NGLDM_Coarseness$_{PET}$ (PET Coarseness from neighborhood gray-level difference matrix) were extracted from the PET dataset. The ICC of the radiomic signatures was all above 0.75. Included MTV, we calculated the Pearson correlation coefficient
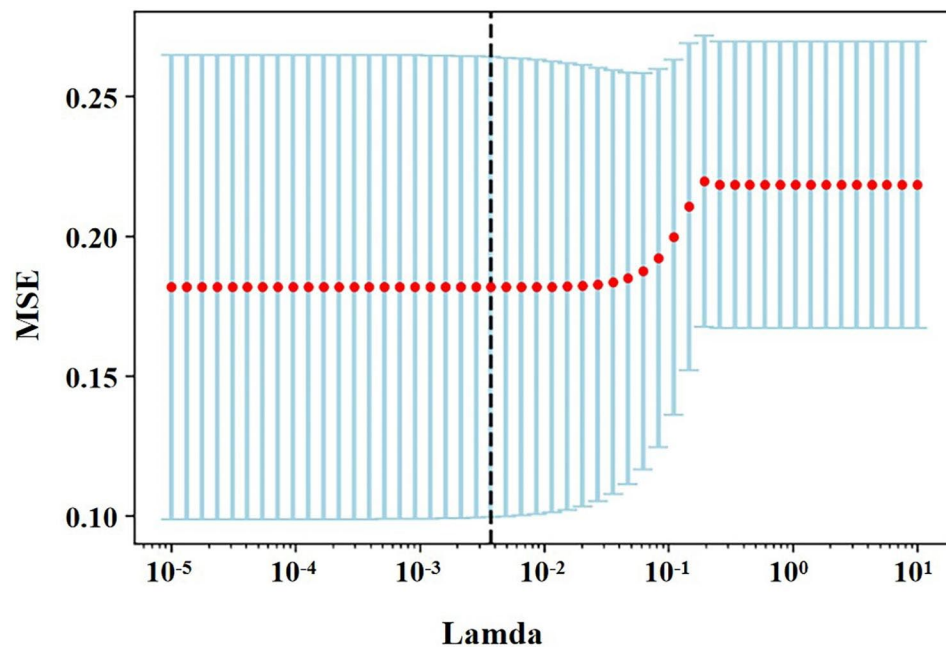
Fig. 2 The Lamda of LASSO regression. The least absolute shrinkage and selection operator (LASSO) was conducted to select the radiomic features of CT and PET. Using 10-fold cross-validation, the suitable value of tuning parameter Lambda (λ) in LASSO regression was selected, and a vertical line was drawn here. MSE: mean squared error

between these features. Figure 3 displays the Pearson correlation coefficient matrix heatmap.

Model construction

In the univariate analysis, the potential meaningful factors were selected for further multivariable regression analysis (p<0.20) [22]. In order to prevent the omission of possible associated factors, those with P<0.15 were included in our multivariate analysis. In addition, ER and PR have been confirmed to be correlated with AR expression in other research, and thus they were also included in our multivariable analysis [23]. Based on the above risk factors, we developed a nomogram capable of predicting the AR expression (Fig. 4). According to the cutoff of the ROC curve, continuous variables were transformed into binary variables (Table 3). It was worth mentioning that high MTV might be related to the negative expression of AR (Fig. 5). Moreover, these lesions were similar on PET/CT images but showed significant differences in the histograms of the radiomic features. Based on binary logistic regression, a diagnostic model consisting of significant risk factors was constructed, including MTV, SHAPE_Sphericity$_{CT}$, and GLCM_Contrast$_{CT}$ (Table 4). GLCM_Contrast$_{CT}$ with a significant statistical difference between the AR+ and AR- (OR [odds ratio]: 1.420; 95% CI [confidence interval]: 9.000 [1.460−55.478]; P=0.018) groups was the independent predictive factor by using the Forward stepwise regression method.

Model effectiveness evaluation

Figure 6 A shows the ROC curve of the combined prediction model. The AUC of the combined model for predicting the AR+was 0.832 (95% CI: 0.697−0.924). The sensitivity and specificity were 75.76% and 80.0%, respectively. Subsequently, 10-fold cross-validation was used to verify the stability of the AUC. The mean value of AUC was 0.833. After bootstrap resampling, we got the calibration curve (Fig. 6B). The concordance index (c-index) of this calibration curve was 0.885 (95%CI: 0.805−0.965), which was reduced to 0.882 after the bias correction. The p-value of the H-L test was beyond 0.05. These results all provided a higher calibration of this model. Finally, the DCA of this study displayed that more benefits could be added to clinical strategies when this prediction model was used to predict the AR expression (Fig. 6C).

Discussion

Some studies have focused on the correlation between the status of other receptors and the extensive expression of AR, indicating that it can promote the proliferation of cancer cells [24]. Accumulating preclinical and clinical evidence supports that some patients can benefit from AR inhibitor therapy, which especially improves the prognosis of TNBC patients [25−27]. In order to avoid the limitations of IHC, recent studies have demonstrated the feasibility of radiomics combined with clinical data for predicting intrinsic molecular subtypes and the expressions of receptors in BC [28, 29]. However, only very few studies have focused on predicting the expression of AR
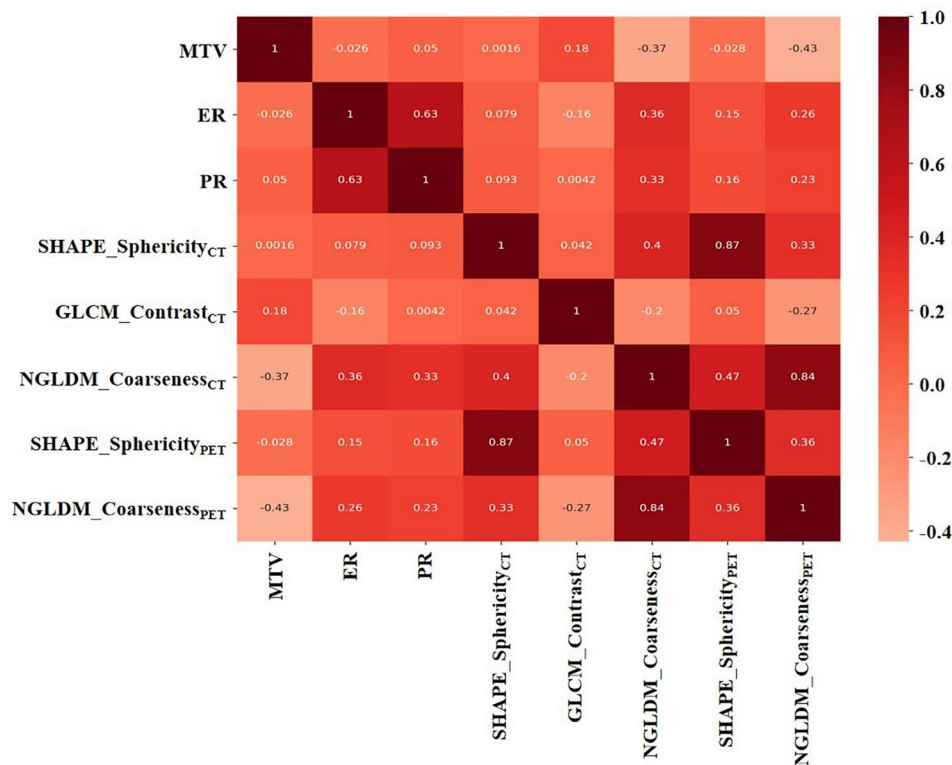
Fig. 3 The Pearson correlation coefficient matrix heatmap in the prediction of AR expression. The darker color presents a higher correlation between the two factors
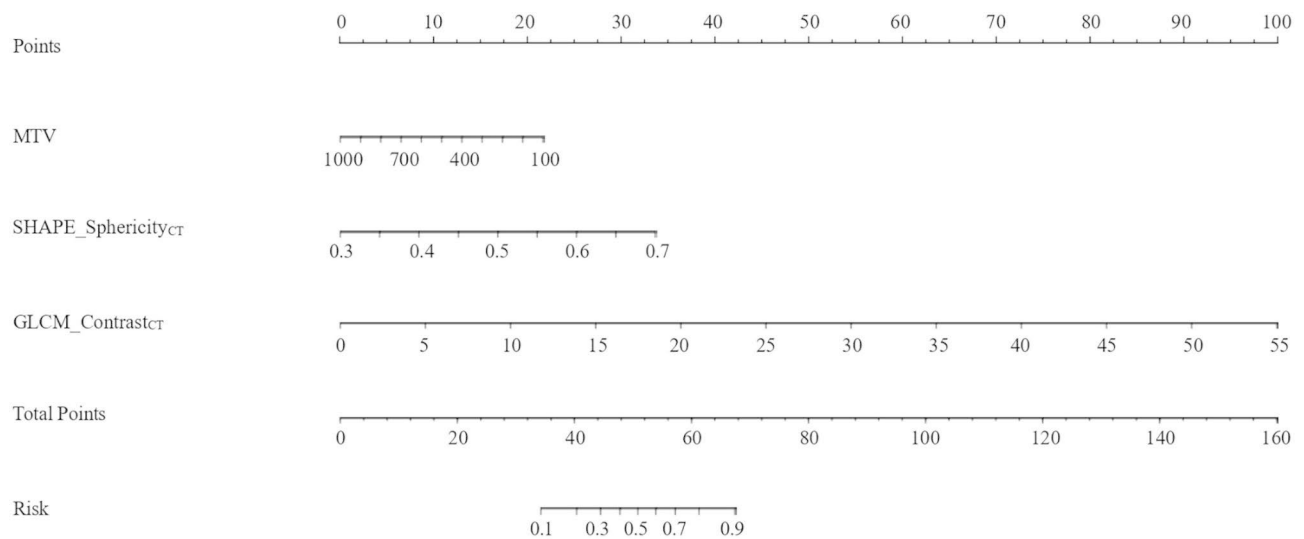

Fig. 4 The nomogram of risk factors predicting the expression of AR. The importance of each variable that established the diagnostic model was visualized as the points

status. In our present study, MTV, SHAPE_Sphericity$_{CT}$, GLCM_Contrast$_{CT}$ extracted from ^{18}F-FDG PET/CT could predict the AR status in BC patients. We further developed a machine-learning model with a higher AUC score on the ROC curve (0.832, 95% CI: 0.697–0.924).

Previous studies have shown that standard parameters (SUV$_{max}$, SUV$_{mean}$, and MTV) extracted from PET images are associated with ER or PR status [17, 30, 31]. In our univariate analysis, there was no obvious correlation between SUV$_{max}$, SUV$_{mean}$, and AR status. Huang et al. have concluded that ER and PR status have significant differences between AR+ and AR- groups [23]. ER and PR status were weakly correlated with the expression of AR (p=0.061, p=0.127)

Jia *et al. BMC Medical Imaging*   (2023) 23:93

Page 8 of 11

Table 3 ROC analyses for meaningful risk factors

Features	AUC (95% CI)	cutoff	p	Se (%)	Sp (%)
SHAPE_Sphericity$_{CT}$	0.747 (0.601–0.862)	> 0.6152	0.0010*	39.39	100.00
GLCM_Contrast$_{CT}$	0.673 (0.522–0.801)	> 7.3826	0.0346*	78.79	60.00
NGLDM_Coarseness$_{CT}$	0.691 (0.541–0.816)	> 0.0020	0.0113*	45.45	100.00
SHAPE_Sphericity$_{PET}$	0.739 (0.593–0.855)	> 0.7362	0.0017*	51.52	86.67
NGLDM_Coarseness$_{PET}$	0.653 (0.501–0.784)	> 0.0431	0.0587	39.39	100.00
MTV	0.695 (0.545–0.820)	≤ 13.1048	0.0096*	45.45	100.00

ROC, receiver operating characteristic; AUC, the area under the curve; Se, Sensitivity; Sp, Specificity. *p < 0.05

Table 4 The Univariable and multivariate analysis of this prediction model

Variable	Uni-p	Multi-p	OR (95%CI)
MTV ≤ 13.1048	0.002*	0.998	
ER status	0.127		
PR status	0.061		
SHAPE_Sphericity$_{CT}$ > 0.6152	0.004*	0.998	
GLCM_Contrast$_{CT}$ > 7.3826	0.008*	0.018*	9.000 (1.460-55.478)
NGLDM_Coarseness$_{CT}$ > 0.0020	0.008*		
SHAPE_Sphericity$_{PET}$ > 0.7362	0.012*		
NGLDM_Coarseness$_{PET}$ > 0.0431	0.004*		

*p < 0.05. Previous continuous variables were transformed into binary variables and then analyzed by the Chi-square test in the Univariable analysis. OR (odds ratio) with its 95% CI was used to estimate correlation strength

in our study. The reason was attributed to the residual confounding factors, and it needs to be further investigated in a larger cohort population [32, 33]. However, high MTV showed a tendency to be associated with AR negativity (p=0.032). Kaida et al. have also found a similar situation, in which a feeble correlation exists between high MTV and ER-negative status [31]. In

further textural analysis, SHAPE_Sphericity$_{CT}$ (p=0.004), GLCM_Contrast$_{CT}$ (p=0.008), NGLDM_Coarseness$_{CT}$ (p=0.008), SHAPE_Sphericity$_{PET}$ (p=0.012), and NGLDM_Coarseness$_{PET}$ (p=0.004) selected by LASSO and t-test were correlated with the expression of AR. In multivariable logistic analysis, only SHAPE_Sphericity$_{CT}$ and GLCM_Contrast$_{CT}$ were included in the prediction model. Due to the limited density resolution of the PET images, they performed worse than CT images in screening and extracting meaningful radiomics signatures [34]. Currently, GLCM (grey-level co-occurrence matrix) textural features are used to classify the tumor grade of BC
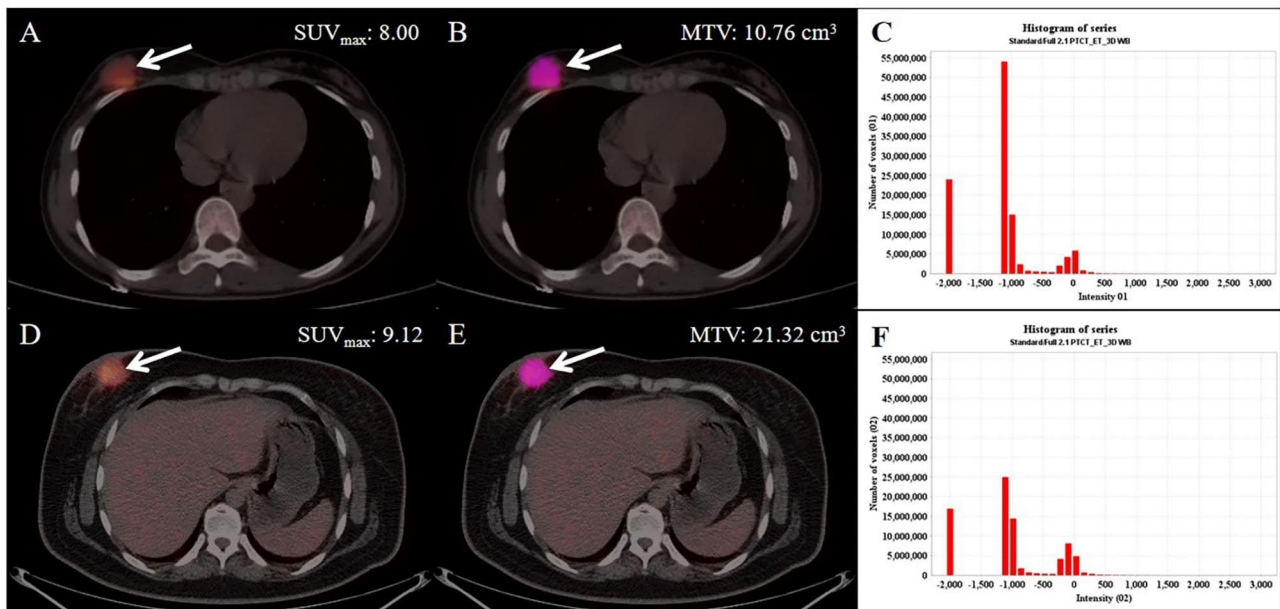

Fig. 5 A typical case of the relationship between MTV and AR expression. Two patients were diagnosed with IDC (invasive ductal breast carcinoma) successively in a year. The former (**A**: PET/CT fusion image, **B**: The VOI of the lesion, **C**: The histogram of VOI) was confirmed as AR-positive (SUV$_{max}$: 8.00; MTV: 10.76 cm^3). The latter (**D**: PET/CT fusion image, **E**: The VOI of the lesion, **F**: The histogram of VOI) was confirmed as AR negative (SUV$_{max}$: 9.12; MTV: 21.32 cm^3). These lesions were similar on PET/CT images but showed significant differences in the histograms of the radiomic features
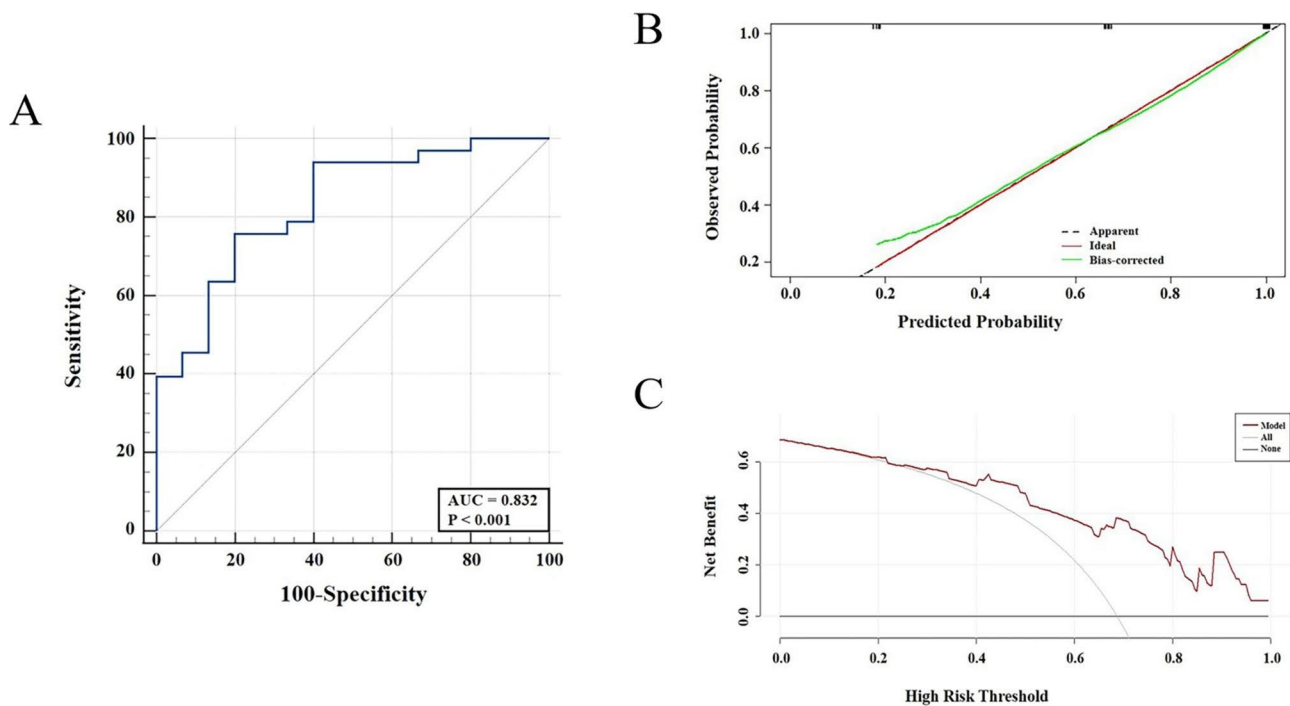
Fig. 6 The evaluation of the prediction model of AR expression in internal validation using Bootstrap. The ROC curve of the combined model consisted of radiomic features and clinical characters (**A**); the calibration curve (green) after correction of bias fluctuates around the ideal curve (red), which revealed the good accuracy between the actual probability and predicted probability (**B**); decision curve showed that the prediction model led to a higher net benefit than intervention or no-intervention of all patients among a large range of threshold (**C**)

[35–38]. Here, we are the first to report the independent performance of $GLCM\_Contrast_{CT}$ in predicting AR molecular markers (p=0.018).

Based on the forward stepwise logistic regression, we established a combined model, in which the accuracy was usually assessed by discrimination, calibration, and clinical applicability [39, 40]. According to its AUC (AUC=0.832), this model presented a better efficacy in the discrimination of AR status. Cross-validation and Bootstrap have proved to be used for the predictive performance of a small sample [41]. Furthermore, using the above methods for internal validation, we finally obtained a very stable value of AUC (AUC=0.833). Some studies have proved that the c-index, with its 95% CI, can provide a more comprehensive assessment of calibration [42, 43]. Combined with the p-value of the H-L test, our model showed a higher capacity for stability [44]. DCA can be used to map the utility of a net benefit assessment model in decision-making within a clinically reasonable risk threshold [45]. The DCA curve of this study visualized that the diagnostic model achieved better net benefit than the all-intervention or no-intervention strategy within a larger threshold range, further proving the excellent clinical applicability of this model.

To the best of our knowledge, we originally established a combined model to predict AR expression based on ^{18}F-FDG PET/CT imaging. There were some limitations in our present study due to the single-center and retrospective design. Next, due to the novelty of the molecular receptor detection of AR, the number of patients included in this study was relatively small. Thirdly, except for internal validation, the resulting model needed to be validated with an external cohort to improve the confidence of clinical applicability. Lastly, a classical supervised classification algorithm should be used to construct a prediction model, and deep learning-based features from PET/CT images need to be verified in further studies.

Conclusions
In conclusion, by combining clinicopathological factors and radiomic features extracted from ^{18}F-FDG PET/CT images, we established a model to predict AR expression in BC patients with a single primary lesion. Our model could serve as a novel strategy to select patients who could benefit from anti-AR treatment and to assist clinicians in making clinical decisions.

Authors' contributions
TJ, QL, BZ, and SD conceptualized and designed the study. CY and SS performed analysis. CY and SD interpreted the data. TJ and QL drafted the manuscript. SS and SD revised the manuscript. All authors contributed to

Jia *et al. BMC Medical Imaging*   (2023) 23:93

Page 10 of 11

Data availability
The original contributions presented in the study are included in the article. Further inquiries can be directed to the corresponding authors.

Declarations

Ethics approval and consent to participate
The studies involving human participants were reviewed and approved by the First Affiliated Hospital of Soochow University. This study was also in accordance with the 1964 Helsinki Declaration and its later amendments or comparable ethical standards. The informed consent was waived by the First Affiliated Hospital of Soochow University because of its retrospective nature. Written informed consent for participation was not required for this study in accordance with national legislation and institutional requirements.

Consent for publication
Not applicable.

Competing interests
The authors declare that the research was conducted in the absence of any commercial or financial relationships that could be construed as a potential conflict of interest.

Author details
¹Department of Nuclear Medicine, The First Affiliated Hospital of Soochow University, Suzhou 215006, China
²Department of General Surgery, The First Affiliated Hospital of Soochow University, Suzhou 215006, China
³Department of Nuclear Medicine, Affiliated Hospital of Jiangnan University, Wuxi 214122, China

References

1. Sung H, Ferlay J, Siegel RL, et al. Global Cancer Statistics 2020: GLOBOCAN estimates of incidence and Mortality Worldwide for 36 cancers in 185 countries. CA Cancer J Clin. 2021;71(3):209–49.
2. Torre LA, Islami F, Siegel RL, Ward EM, Jemal A. Global Cancer in Women: Burden and Trends. Cancer Epidemiol Biomarkers Prev. 2017;26(4):444–57.
3. Zardavas D, Irrthum A, Swanton C, Piccart M. Clinical management of breast cancer heterogeneity. Nat Rev Clin Oncol. 2015;12(7):381–94.
4. Yeo SK, Guan JL. Breast Cancer: multiple subtypes within a Tumor? Trends Cancer. 2017;3(11):753–60.
5. Harbeck N, Gnant M. Breast cancer. Lancet. 2017;389(10074):1134–50.
6. Clarke R, Tyson JJ, Dixon JM. Endocrine resistance in breast cancer–An overview and update. Mol Cell Endocrinol. 2015;418(03):220–34.
7. Maximiano S, Magalhães P, Guerreiro MP, Morgado M. Trastuzumab in the treatment of breast Cancer. BioDrugs. 2016;30(2):75–86.
8. Bianchini G, Balko JM, Mayer IA, Sanders ME, Gianni L. Triple-negative breast cancer: challenges and opportunities of a heterogeneous disease. Nat Rev Clin Oncol. 2016;13(11):674–90.
9. Collins LC, Cole KS, Marotti JD, Hu R, Schnitt SJ, Tamimi RM. Androgen receptor expression in breast cancer in relation to molecular phenotype: results from the Nurses' Health Study. Mod Pathol. 2011;24(7):924–31.
10. Yu Q, Niu Y, Liu N, et al. Expression of androgen receptor in breast cancer and its significance as a prognostic factor. Ann Oncol. 2011;22(6):1288–94.
11. Robinson JL, Macarthur S, Ross-Innes CS, et al. Androgen receptor driven transcription in molecular apocrine breast cancer is mediated by FoxA1. EMBO J. 2011;30(15):3019–27.
12. Rechoum Y, Rovito D, Iacopetta D, et al. AR collaborates with ERα in aromatase inhibitor-resistant breast cancer. Breast Cancer Res Treat. 2014;147(3):473–85.
13. Ni M, Chen Y, Lim E, et al. Targeting androgen receptor in estrogen receptor-negative breast cancer. Cancer Cell. 2011;20(1):119–31.
14. Ni M, Chen Y, Fei T, et al. Amplitude modulation of androgen signaling by c-MYC. Genes Dev. 2013;27(7):734–48.
15. Lehmann BD, Bauer JA, Chen X, et al. Identification of human triple-negative breast cancer subtypes and preclinical models for selection of targeted therapies. J Clin Invest. 2011;121(7):2750–67.
16. Masuda H, Baggerly KA, Wang Y, et al. Differential response to neoadjuvant chemotherapy among 7 triple-negative breast cancer molecular subtypes. Clin Cancer Res. 2013;19(19):5533–40.
17. Antunovic L, Gallivanone F, Sollini M, et al. [18F] FDG PET/CT features for the molecular characterization of primary breast tumors. Eur J Nucl Med Mol Imaging. 2017;44(12):1945–54.
18. Groheux D, Cochet A, Humbert O, Alberini JL, Hindié E, Mankoff D. ¹⁸F-FDG PET/CT for staging and restaging of breast Cancer. J Nucl Med. 2016;57(Suppl 1):17S–26S.
19. Ulaner GA. PET/CT for patients with breast Cancer: where is the clinical impact? AJR Am J Roentgenol. 2019;213(2):254–65.
20. Valdora F, Houssami N, Rossi F, Calabrese M, Tagliafico AS. Rapid review: radiomics and breast cancer. Breast Cancer Res Treat. 2018;169(2):217–29.
21. Nioche C, Orlhac F, Boughdad S, Reuzé S, Goya-Outi J, Robert C, Pellot-Barakat C, Soussan M, Frouin F, Buvat I. LIFEx: a freeware for radiomic feature calculation in multimodality imaging to accelerate advances in the characterization of tumor heterogeneity. Cancer Res. 2018;78(16):4786–9.
22. Bouwman L, Eeltink CM, Visser O, Janssen JJWM, Maaskant JM. Prevalence and associated factors of medication non-adherence in hematological-oncological patients in their home situation. BMC Cancer. 2017;17(1):739.
23. Huang Y, Wei L, Hu Y, et al. Multi-parametric MRI-Based Radiomics Models for Predicting Molecular Subtype and Androgen receptor expression in breast Cancer. Front Oncol. 2021;11:706733.
24. Kono M, Fujii T, Lim B, Karuturi MS, Tripathy D, Ueno NT. Androgen receptor function and androgen receptor-targeted therapies in breast Cancer: a review. JAMA Oncol. 2017;3(9):1266–73.
25. Gerratana L, Basile D, Buono G, et al. Androgen receptor in triple negative breast cancer: a potential target for the targetless subtype. Cancer Treat Rev. 2018;68:102–10.
26. Anestis A, Karamouzis MV, Dalagiorgou G, Papavassiliou AG. Is androgen receptor targeting an emerging treatment strategy for triple negative breast cancer? Cancer Treat Rev. 2015;41(6):547–53.
27. Shi Y, Yang F, Huang D, Guan X. Androgen blockade based clinical trials landscape in triple negative breast cancer. Biochim Biophys Acta Rev Cancer. 2018;1870(2):283–90.
28. Pinker K, Chin J, Melsaether AN, Morris EA, Moy L. Precision Medicine and Radiogenomics in breast Cancer: New Approaches toward diagnosis and treatment. Radiology. 2018;287(3):732–47.
29. Liu Z, Wang S, Dong D, et al. The applications of Radiomics in Precision diagnosis and treatment of Oncology: Opportunities and Challenges. Theranostics. 2019;9(5):1303–22.
30. Gallivanone F, Canevari C, Sassi I, et al. Partial volume corrected 18F-FDG PET mean standardized uptake value correlates with prognostic factors in breast cancer. Q J Nucl Med Mol Imaging. 2014;58(4):424–39.
31. Kaida H, Toh U, Hayakawa M, et al. The relationship between 18F-FDG metabolic volumetric parameters and clinicopathological factors of breast cancer. Nucl Med Commun. 2013;34(6):562–70.
32. Zwanenburg A. Radiomics in nuclear medicine: robustness, reproducibility, standardization, and how to avoid data analysis traps and replication crisis. Eur J Nucl Med Mol Imaging. 2019;46(13):2638–55.
33. Zhou Y, Li J, Zhang X, et al. Prognostic value of Radiomic features of 18F-FDG PET/CT in patients with B-Cell lymphoma treated with CD19/CD22 dual-targeted chimeric Antigen receptor T cells. Front Oncol. 2022;12:834288.

34. Li J, Ge S, Sang S, Hu C, Deng S. Evaluation of PD-L1 expression level in patients with Non-Small Cell Lung Cancer by 18F-FDG PET/CT Radiomics and Clinicopathological characteristics. Front Oncol. 2021;11:789014.

35. Schiano C, Franzese M, Pane K, et al. Hybrid 18F-FDG-PET/MRI measurement of standardized uptake value coupled with Yin Yang 1 signature in metastatic breast Cancer. A preliminary study. Cancers (Basel). 2019;11(10):1444.

36. Grueneisen J, Sawicki LM, Wetter A, et al. Evaluation of PET and MR datasets in integrated 18F-FDG PET/MRI: a comparison of different MR sequences for whole-body restaging of breast cancer patients. Eur J Radiol. 2017;89:14–9.

37. Rahim MK, Kim SE, So H, et al. Recent Trends in PET Image Interpretations using volumetric and texture-based quantification methods in Nuclear Oncology. Nucl Med Mol Imaging. 2014;48(1):1–15.

38. Chang CC, Cho SF, Chen YW, Tu HP, Lin CY, Chang CS. SUV on dual-phase FDG PET/CT correlates with the Ki-67 proliferation index in patients with newly diagnosed non-hodgkin lymphoma. Clin Nucl Med. 2012;37(8):e189–95.

39. Kramer AA, Zimmerman JE. Assessing the calibration of mortality benchmarks in critical care: the Hosmer-Lemeshow test revisited. Crit Care Med. 2007;35(9):2052–6.

40. Vickers AJ, Van Calster B, Steyerberg EW. Net benefit approaches to the evaluation of prediction models, molecular markers, and diagnostic tests. BMJ. 2016;352:i6.

41. Steyerberg EW, Bleeker SE, Moll HA, Grobbee DE, Moons KG. Internal and external validation of predictive models: a simulation study of bias and precision in small samples. J Clin Epidemiol. 2003;56(5):441–7.

42. Iasonos A, Schrag D, Raj GV, Panageas KS. How to build and interpret a nomogram for cancer prognosis. J ClinOncol. 2008;26(8):1364–70.

43. Pencina MJ, D'Agostino RB. Overall C as a measure of discrimination in survival analysis: model specific population value and confidence interval estimation. Stat Med. 2004;23(13):2109–23.

44. Bertolini G, D'Amico R, Nardi D, Tinazzi A, Apolone G. One model, several results: the paradox of the Hosmer-Lemeshow goodness-of-fit test for the logistic regression model. J Epidemiol Biostat. 2000;5(4):251–3.

45. Van Calster B, Wynants L, Verbeek JFM, et al. Reporting and interpreting decision curve analysis: a guide for investigators. Eur Urol. 2018;74(6):796–804.

Publisher's Note